

A Simplified Sub-Nyquist Receiver Architecture for Joint DOA and Frequency Estimation

Liang Liu and Ping Wei

Abstract—Joint estimation of carrier frequency and direction of arrival (DOA) for multiple signals has been found in many practical applications such as Cognitive Radio (CR). However, Nyquist sampling mechanism is costly or implemented due to wide spectrum range. Taking advantage of sub-Nyquist sampling technology, some array receiver architectures are proposed to realize joint estimation of carrier frequency and DOA. To further decrease equivalent sampling rate and hardware complexity, we propose a simplifying receiver architecture based on our previous work. We come up with joint DOA and frequency estimation algorithms for the novel architecture. The simulations demonstrate that the receiver architecture and the proposed approaches are feasible.

Index Terms—Direction-of-arrival estimation, frequency estimation, sub-Nyquist sampling.

I. INTRODUCTION

NOWADAYS, both carrier frequency and direction of arrival (DOA) are needed in some applications, such as Cognitive Radio (CR) aiming at solving the spectral congestion [1]–[5]. The most important function of CRs is to autonomously exploit locally unused spectrum to provide new paths to spectrum access. Therefore, spectrum sensing is an essential part of CRs. The conventional spectrum opportunity only contains three dimensions of the spectrum space: frequency, time, and space. However, with the advancement in array processing technologies [6]–[8], the new dimension, DOA, also creates new spectrum opportunities. Joint frequency spectrum and spatial spectrum would enhance the performance of CRs.

Recently, significant effort have been made towards jointly estimation of carrier frequencies and their DOAs [9], [10]. An obvious drawback is that they require additional pairing between the carrier frequencies and the DOAs. Besides, both works assume that the signal is sampled at least at its Nyquist rate. The main challenge of CRs lies in wideband signal processing for their costly or even unreachable Nyquist rate sampling. The distribution range of the spectrum under monitoring is from 300 MHz to several GHz [1]–[5]. It leads to high Nyquist sampling rate and a large number of sampling data to process.

Fortunately, sub-Nyquist sampling technology can reconstruct a multiband signal from its sub-Nyquist samples [11]–[14]. Latterly, some joint DOA and carrier frequency estimation methods are proposed at sub-Nyquist sampling rates. [15]

proposes a structure, i.e. a linear array by employing a multi-coset sampling at the output of every sensor. This method compresses the wide-sense stationary signal in both the time domain and spatial domain. To simplify the hardware complexity, [16] uses an additional identical delayed channel at the output of every sensor. But there are ambiguities during pairing with their corresponding DOAs in an underlying uniform linear array (ULA) scenario. To solve the pairing issue, [17] proposes a structure with the hardware complexity identical to that of [16]. However, those papers do not give a unified signal reception model. [18] presents two joint DOA and carrier frequency recovery approaches for an L-shaped ULA scenario. In [19], we propose a new array receiver architecture associated with two sub-Nyquist sampling based methods for simultaneously estimate the frequencies and DOAs of multiple narrowband far-field signals impinging on a ULA, where signals carrier frequencies spread around the whole wide spectrum. The architecture is complex due to every sensor following a multi-channel sub-Nyquist sampling receiver.

We consider a scene as [19] in this paper. For reducing the complexity of receiver, we propose a simplified array receiver architecture. For this model, we propose a unified formula and methods for joint estimation of DOA and carrier frequency.

The following notations are used in the paper. $(\cdot)^T$ and $(\cdot)^H$ denote the transpose and Hermitian transpose, respectively. $E(\cdot)$ stands for the expectation operator. x_j is the j th entry of a vector \mathbf{x} . \mathbf{A}_i and A_{ij} are the i th column and (i, j) th entry of a matrix \mathbf{A} , respectively. \otimes denotes the Hadamard product. \mathbf{I}_M stands for an $M \times M$ identity matrix.

II. ARRAY SIGNAL MODEL WITH SUB-NYQUIST SAMPLING

In [19], we proposed an array signal receiver architecture and the corresponding signal reception model, which introduces sub-Nyquist sampling technology. In this letter, on one hand, the proposed architecture is the simplified form of the previous architecture, on the other hand, we will take advantage of the previous model when estimation algorithm deducing. Therefore, we review the main conclusions of [19] in this section.

Consider K narrowband far-field signals impinging on a ULA composed of M ($M > K$) sensors. Our previous receiver architecture applies multi-coset sampling [14]. And every array sensor is followed by same P delay branches. All the ADCs are synchronized and samples at a sub-Nyquist sampling rate of $f_s = f_N/L$, where $f_N = 1/T_N$ is the Nyquist sampling rate. The constant set $C = [c_1, c_2, \dots, c_P]$ is the

The authors are with the Center for Cyber Security, School of Electronic Engineering, University of Electronic Science and Technology of China, Chengdu 611731, China (e-mail: liu_yinliang@outlook.com; pwei@uestc.edu.cn).

sampling pattern where $0 \leq c_1 < c_2 < \dots < c_P \leq L - 1$. $y_{mp}[n]$ denotes the sampled signal corresponding to the m th sensor, p th branch. The matrix output of all branches of all sensors is given by

$$\mathbf{Y}(f) = (\mathbf{A} \otimes \mathbf{B}) \bar{\mathbf{S}}(f) + (\mathbf{I}_M \otimes \mathbf{B}) \hat{\mathbf{N}}(f) \quad (1)$$

$$\triangleq \mathbf{G} \bar{\mathbf{S}}(f) + \mathbf{I}_B \hat{\mathbf{N}}(f), f \in \mathcal{F} \triangleq \left[0, \frac{1}{LT}\right), \quad (2)$$

where $B_{il} = \frac{1}{\sqrt{L}} \exp(j \frac{2\pi}{L} c_i l)$, $A_{mk} = \exp(-j \phi_k (m - 1))$ is the mk th element of the steer array \mathbf{A} , where spatial phase

$$\phi_k = \frac{2\pi d \sin(\theta_k)}{c/f_k}, \quad (3)$$

where θ_k and f_k are the DOA and the center frequency of $s_k(t)$, respectively. $\bar{\mathbf{S}}(f) = [\bar{\mathbf{S}}_1^T(f), \bar{\mathbf{S}}_2^T(f), \dots, \bar{\mathbf{S}}_K^T(f)]^T$, $\bar{\mathbf{S}}_k(f) = [S_{k1}(f), S_{k2}(f), \dots, S_{kL}(f)]^T$, $S_{kl}(f) = S_k(f + \frac{l-1}{LT})$, $S_k(f)$ is the Fourier transform of $s_k(t)$. $\mathbf{s}(t) = [s_1(t), s_2(t), \dots, s_K(t)]^T$ is the vector of all signal values. Because $s_k(t)$ is a narrowband signal, there is one, and only one frequency band which is occupied in $\bar{\mathbf{S}}_k(f)$. Further, $\bar{\mathbf{S}}_k(f)$ is a sparse vector of length L when k is fixed and there is one, and only one index (marked as l_k), which is activated. $\mathbf{Y}(f) = [\mathbf{Y}_1^T(f), \mathbf{Y}_2^T(f), \dots, \mathbf{Y}_M^T(f)]^T$. The p th element of $\mathbf{Y}_{mp}(f) = \sqrt{LT_N} Y_{mp}(e^{j2\pi f T})$, which is the discrete-time Fourier transform of the signal $y_{mp}[n]$ except a coefficient difference $\sqrt{LT_N}$. $\hat{\mathbf{N}}(f) = [\hat{\mathbf{N}}_1^T(f), \dots, \hat{\mathbf{N}}_M^T(f)]^T$, $\hat{\mathbf{N}}_m(f) = [N_{m1}(f), \dots, N_{mL}(f)]^T$, $N_{kl}(f) = N_k f + \frac{l-1}{LT}$ is the Fourier transform of $n_k(t)$. $\mathbf{n}(t) = [n_1(t), \dots, n_M(t)]^T$ is the noise vector, which subjects to the zero-mean circular complex Gaussian distribution with covariance matrix $\sigma^2 \mathbf{I}_M$.

III. PROPOSED RECEIVER ARCHITECTURE AND JOINT DOA AND FREQUENCY ESTIMATION ALGORITHM

A. Proposed receiver architecture

To largely decrease hardware complexity, we design the simplified receiver architecture when achieving joint frequency and DOA estimate. This architecture is set up based on the previous architecture. The main difference between the two architectures is that the former only reserves all branches of one array sensor and whole same branch of all sensors. The proposed receiver architecture is shown in Fig.1. Without loss of generality, we select all branches of the first sensor and whole first branch of all sensors in the Fig.1. Namely, our output is $\mathbf{W}(f) = [Y_{11}(f), Y_{12}(f), \dots, Y_{1P}(f), Y_{21}(f), \dots, Y_{M1}(f)]^T$. We define a $(M + P - 1) \times MP$ matrix \mathbf{J} , where $J_{ij} = 1$ for $i = 1, \dots, P$, and $j = i$; or $i = P + 1, \dots, M + P - 1$, and $j = 1 + iP - P^2$; else $J_{ij} = 0$ for else. We have $\mathbf{W}(f) = \mathbf{JY}(f)$. According to (1), we have

$$\mathbf{W}(f) = \mathbf{H} \bar{\mathbf{S}}(f) + \mathbf{J} \mathbf{I}_B \hat{\mathbf{N}}(f), f \in \mathcal{F}, \quad (4)$$

where $\mathbf{H} = \mathbf{J}(\mathbf{A} \otimes \mathbf{B}) = \mathbf{JG}$. Combing $\mathbf{I}_{MP} = \mathbf{I}_B \mathbf{I}_P^H$ in [19], we have

$$\mathbf{J} \mathbf{I}_B \hat{\mathbf{N}}(f) \left(\mathbf{J} \mathbf{I}_B \hat{\mathbf{N}}(f) \right)^H = \sigma^2 \mathbf{I}_{M+P-1}. \quad (5)$$

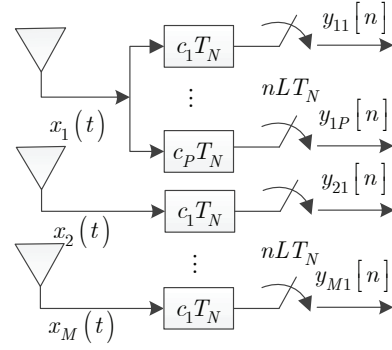


Fig. 1. Proposed receiver architecture.

B. Algorithm Based on Individual Estimate

1) *Spatial Phase Estimate*: We denote the outputs of the 1st branch of all sensors as $\mathbf{Q}(f) = [\mathbf{Y}_{11}(f) \dots \mathbf{Y}_{M1}(f)]^T$. According to [19], we have the following equation.

$$\mathbf{Q}(f) = \mathbf{AZ}(f) + \hat{\mathbf{N}}_1(f), \quad (6)$$

where $\mathbf{Z}(f) = \left[\sum_{l=1}^L B_{1l} S_{1l}(f) \dots \sum_{l=1}^L B_{1l} S_{Kl}(f) \right]^T$. Because $\mathbf{S}_k(f)$ is a 1-sparse vector of length L , and the activated index is l_k . We can simplify $\mathbf{Z}(f)$ as $\mathbf{Z}(f) = [B_{1l_1} S_{1l_1}(f) \dots B_{1l_K} S_{Kl_K}(f)]^T$. (6) is a standard array reception model, there are many existing method to get ϕ , such as MUSIC, ESPRIT, and so on. Further, we can get the least square solution of $\mathbf{Z}(f)$,

$$\mathbf{Z}(f) = \mathbf{A}^\dagger \mathbf{Q}(f). \quad (7)$$

2) *Frequency Estimate*: According to [19] section III part B, the output of all branches of the 1st sensor is

$$\mathbf{Y}_1(f) = \mathbf{B} \bar{\mathbf{X}}_1(f), \quad (8)$$

where $\bar{\mathbf{X}}_1(f) = \left[\sum_{k=1}^K A_{1k} S_{k1}(f) \dots \sum_{k=1}^K A_{1k} S_{kL}(f) \right]^T$. Since $\mathbf{S}_k(f)$ is a 1-sparse vector of length L , $\bar{\mathbf{X}}_1(f)$ is K -sparse vector of length L . We denote the support set of $\bar{\mathbf{X}}_1(f)$ as Ω . We can use the CTF algorithm to solve (8) to obtain Ω . Then, we hold

$$\bar{\mathbf{Y}}_1(f) = \mathbf{B} \bar{\mathbf{X}}_1(f) = \mathbf{B}_\Omega (\bar{\mathbf{X}}_1)_\Omega(f). \quad (9)$$

Further, we can get the least square solution of $(\bar{\mathbf{X}}_1)_\Omega(f)$,

$$(\bar{\mathbf{X}}_1)_\Omega(f) = \mathbf{B}_\Omega^\dagger \bar{\mathbf{Y}}_1(f). \quad (10)$$

3) *Spatial Phase and Frequency matching algorithm*: We calculate the cross-correlation function of signal estimates $\mathbf{Z}(f)$ and $(\bar{\mathbf{X}}_1)_\Omega(f)$. The absolute value of the cross-correlation matrix element has the following expression

TABLE I
ALGORITHM JDFPI

- 1) According to (6), obtain ϕ applying the MUSIC, ESPRIT algorithm, and so on;
- 2) Compute $\mathbf{Z}(f)$ according to (7);
- 3) Apply the CTF algorithm to solve (8) to obtain Ω ;
- 4) Compute $(\bar{\mathbf{X}}_1)_\Omega(f)$ according to (10);
- 5) Determine the support index \mathcal{S} according to (14);
- 6) Compute $\bar{\mathbf{S}}_\mathcal{S}(f)$ according to (15);
- 7) Determine \bar{f}_k through $\bar{\mathbf{S}}_\mathcal{S}(f)$ applying the MUSIC, ESPRIT algorithm, and so on;
- 8) Acquire f_k according to (17);
- 9) Calculate θ_k through (3);

$$|R_{ij}| = \left| E \left\{ B_{1l_i} S_{il_i}(f) \left(\sum_{k=1}^K A_{1k} S_{k\Omega_j}(f) \right)^H \right\} \right| \quad (11)$$

$$= \left| E \left\{ S_{kl_k}(f) (S_{k\Omega_j}(f))^H \right\} \right| \quad (12)$$

$$= \begin{cases} > 0, \text{ when } l_i = \Omega_j \\ = 0, \text{ when } l_i \neq \Omega_j \end{cases}, 1 \leq i \leq K, 1 \leq j \leq c. \quad (13)$$

The conditions for the establishment of (12) have the signals are uncorrelated, the magnitudes of both B_{1l_i} and A_{1k} are 1. If any of the two signal frequencies are in different frequency bands, we have $c = K$, or $c < K$. According to (11), we know that there is one absolute value of element is dominant in each row of \mathbf{R} . Further, the support index \mathcal{S} of \mathbf{H} is determined as following:

$$S_i = (i-1)L + \Omega_j, j = \arg \max_j |R_{ij}|, 1 \leq i \leq K. \quad (14)$$

With known the support index \mathcal{S} , we obtain

$$\mathbf{W}(f) = \mathbf{H}\bar{\mathbf{S}}(f) = \mathbf{H}_\mathcal{S}\bar{\mathbf{S}}_\mathcal{S}(f) + \mathbf{J}\mathbf{I}_B\hat{\mathbf{N}}(f), f \in \mathcal{F}. \quad (15)$$

Then we have the least square solution of $\bar{\mathbf{S}}_\mathcal{S}(f)$

$$\bar{\mathbf{S}}_\mathcal{S}(f) = \mathbf{H}_\mathcal{S}^\dagger \mathbf{W}(f). \quad (16)$$

We can gain the received signal's frequency \bar{f}_k through $\bar{\mathbf{S}}_\mathcal{S}(f)$. Besides, there is a relationship between \bar{f}_k and the original signal's frequency f_k ,

$$f_k = (S_k \% L - 1) \frac{f_N}{L} + \bar{f}_k. \quad (17)$$

We can calculate θ_k through (3). We outline the main steps of this individual estimate method for partial channels named algorithm JDFPI in table I.

C. Algorithm Based on subspace decomposition

If we calculate the covariance matrix of $\mathbf{W}(f)$, and take advantage of the subspace decomposition theory as [7], we will have similar conclusion:

$$\mathbf{a}_l(\phi) \perp \mathbf{U}_N, \quad (18)$$

where \mathbf{U}_N is the noise subspace. The difference is $\mathbf{a}_l(\phi) = \mathbf{J}(\mathbf{a}(\phi) \otimes \mathbf{B}_l)$. Similarly, we can execute the steps of Algorithm JDFSD [19]. It is worth pointing out that \mathbf{G} and $\mathbf{Y}(f)$

in [19] need to be replaced by \mathbf{H} and $\mathbf{W}(f)$, respectively. We name this method as algorithm based on subspace decomposition for partial channels (JDFSDPJ).

D. Performance Analysis: Cramér-Rao Bound

Comparing the model (15) and model (11) in [19] and noticing that (5) holds, and making use of the conclusion of Section V equation (29) in [19], we have

$$\begin{aligned} \text{CRB}_{\text{sub}}(\text{sim}) &= \frac{\sigma^2}{2T/L} \left(\Re \left((\mathbf{E}^H \mathbf{P}_{\mathbf{H}_\mathcal{S}} \mathbf{E}) \odot \mathbf{R}_\mathcal{S}^H \right) \right)^{-1} \\ &= \frac{\sigma^2}{2T} \left(\Re \left((\mathbf{E}^H \mathbf{P}_{\mathbf{H}_\mathcal{S}} \mathbf{E}) \odot \mathbf{R}_\mathcal{S}^H \right) \right)^{-1}, \end{aligned} \quad (19)$$

where $\mathbf{P}_{\mathbf{H}_\mathcal{S}} = \mathbf{I} - \mathbf{H}_\mathcal{S} \mathbf{H}_\mathcal{S}^\dagger$, where $\mathbf{H}_\mathcal{S}^\dagger = (\mathbf{H}_\mathcal{S}^H \mathbf{H}_\mathcal{S})^{-1} \mathbf{H}_\mathcal{S}^H$, $\mathbf{E} = [\mathbf{E}_1, \dots, \mathbf{E}_K]$, $\mathbf{E}_i = \frac{d\mathbf{H}_{\mathcal{S}_i}}{d\phi_i}$.

IV. SIMULATION

In this section, we present the numerical simulation results to illustrate the performance of the proposed algorithms. For the sake of comparison, we take JDFSD in [19] as a representative of full structure, as JDFSD and JDFTD have the same performance. We set the receiver structure as [19], and we take the all branches of the 1st sensor and the 1st branch of all sensors as our simplified structure. For the same reason mentioned in [19], we will only give the phase estimation simulation result rather than the DOA estimation simulation result in those simulations.

A. Performance with noise

Firstly, we will show our model can be solved by the proposed algorithm in different noise levels. In this subsection, the simulation scenario is the same as section VI-A in [19].

Fig.2-Fig.3 depict the RMSE versus SNR in terms of spatial phase and frequency estimation, respectively. Fig.2 shows that the phase estimation performance of algorithms JDFSDPJ and JDFPI improves with SNR, where JDFSDPJ achieves the $\text{CRB}_{\text{sub}}(\text{Sim})$. The phase estimation performance of JDFSDPJ is better than that of JDFPI is because of jointly using the information in frequency domain and spatial domain. And we observe that $\text{CRB}_{\text{sub}}(\text{Sim})$ lies between CRB_{sub} and CRB_{Ny} . $\text{CRB}_{\text{sub}}(\text{Sim})$ is higher than CRB_{sub} is obvious. The simplified structure use the jointly information from frequency domain and spatial domain. It leads to a big improvement although the simplified structure have much less samplings comparing with Nyquist sampling. In Fig.3 demonstrates that the frequency estimation performances of JDFSDPJ and JDFPI can achieve the $\text{CRB}_{\text{sub}}(\text{Sim})$, which is certainly higher than $\text{CRB}_{\text{sub}}(\text{Sim})$ because of using less branches.

B. Performance with various signal number

In this subsection, we will investigate the estimation performance when the signal number changes as section VI-C in [19]. Fig.4 shows that the phase (DOA) estimation performance of algorithm JDFSDPJ is slightly influenced by the signal number and achieves $\text{CRB}_{\text{sub}}(\text{Sim})$, however JDFPI is

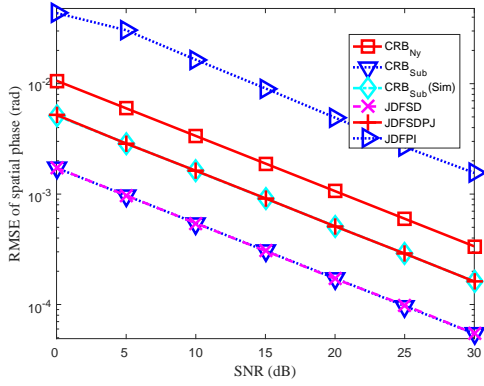


Fig. 2. RMSE of phase estimates versus SNR.

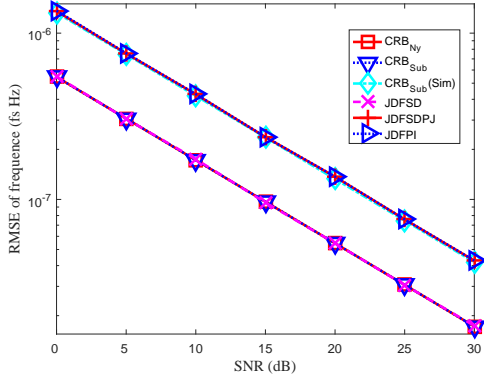


Fig. 3. RMSE of frequency estimates versus SNR.

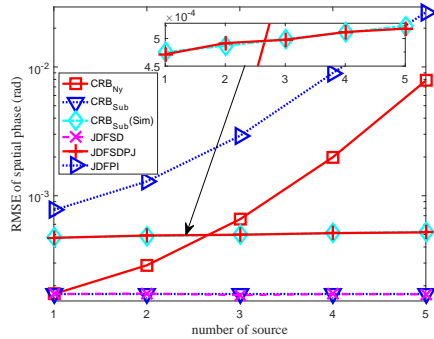


Fig. 4. RMSE of phase estimates versus number of source.

influenced by the signal number. This is due to the former jointly using the information from frequency domain and spatial domain. To some degree, it maintains good robustness in terms of the number of signals as JDFSD. Without doubt the performance of JDFSDPJ is still worse than CRB_{sub} . Fig.5 shows that the frequency estimation performances of algorithms JDFSDPJ and JDFPI are not influenced by the signal number and can reach $CRB_{sub}(Sim)$.

V. CONCLUSIONS

In this paper, we designed an simplified array receiver architecture by introducing sub-Nyquist sampling technology. We realized the joint DOA and frequency estimation under lower sampling rate. Although the estimate precision of using

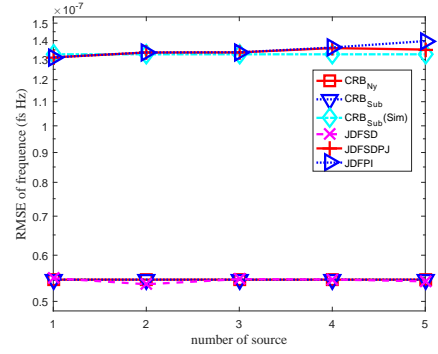


Fig. 5. RMSE of frequency estimates versus number of source.

partial channels is worse than that of using full channels, the former has lower equivalent sampling rate and hardware complexity. And increase time of sensing will enhance its estimation performance. The simulations demonstrated that the joint algorithm can closely match the CRB according to noise levels and source number as well.

REFERENCES

- [1] S. Haykin, "Cognitive radio: brain-empowered wireless communications," *IEEE J. Sel. Areas Commun.*, vol. 23, no. 2, pp. 201–220, Feb 2005.
- [2] T. Yucek and H. Arslan, "A survey of spectrum sensing algorithms for cognitive radio applications," *IEEE Commun. Surveys Tuts.*, vol. 11, no. 1, pp. 116–130, First 2009.
- [3] M. Mishali and Y. C. Eldar, "Wideband spectrum sensing at sub-Nyquist rates [applications corner]," *IEEE Signal Process. Mag.*, vol. 28, no. 4, pp. 102–135, July 2011.
- [4] H. Sun, A. Nallanathan, C. X. Wang, and Y. Chen, "Wideband spectrum sensing for cognitive radio networks: a survey," *IEEE Wireless Commun.*, vol. 20, no. 2, pp. 74–81, April 2013.
- [5] D. Cohen and Y. C. Eldar, "Sub-Nyquist sampling for power spectrum sensing in cognitive radios: A unified approach," *IEEE Trans. Signal Process.*, vol. 62, no. 15, pp. 3897–3910, Aug 2014.
- [6] H. Krim and M. Viberg, "Two decades of array signal processing research: the parametric approach," *IEEE Signal Process. Mag.*, vol. 13, no. 4, pp. 67–94, Jul 1996.
- [7] R. Schmidt, "Multiple emitter location and signal parameter estimation," *IEEE Trans. Antennas Propag.*, vol. 34, no. 3, pp. 276–280, Mar 1986.
- [8] R. Roy, A. Paulraj, and T. Kailath, "ESPRIT—a subspace rotation approach to estimation of parameters of cisoids in noise," *IEEE Trans. Acoust., Speech, Signal Process.*, vol. 34, no. 5, pp. 1340–1342, Oct 1986.
- [9] A. N. Lemma, A. J. van der Veen, and E. F. Deprettere, "Joint angle-frequency estimation using multi-resolution esprit," in *Proc. IEEE Int. Conf. on Acous. Speech and Signal Process. (ICASSP)*, vol. 4, May 1998, pp. 1957–1960 vol.4.
- [10] A. Lemma, A. J. V. der Veen, and E. Deprettere, "Analysis of joint angle-frequency estimation using esprit," *IEEE Trans. Signal Process.*, vol. 51, no. 5, pp. 1264–1283, May 2003.
- [11] M. Mishali and Y. C. Eldar, "Sub-Nyquist sampling," *IEEE Signal Process. Mag.*, vol. 28, no. 6, pp. 98–124, Nov 2011.
- [12] —, "From theory to practice: Sub-Nyquist sampling of sparse wideband analog signals," *IEEE J. Sel. Topics Signal Process.*, vol. 4, no. 2, pp. 375–391, April 2010.
- [13] Y. C. Eldar and T. Michaeli, "Beyond bandlimited sampling," *IEEE Signal Process. Mag.*, vol. 26, no. 3, pp. 48–68, May 2009.
- [14] M. Mishali and Y. C. Eldar, "Blind multiband signal reconstruction: Compressed sensing for analog signals," *IEEE Trans. Signal Process.*, vol. 57, no. 3, pp. 993–1009, March 2009.
- [15] D. D. Ariananda and G. Leus, "Compressive joint angular-frequency power spectrum estimation," in *Proc. Eur. Sig. Process. Conf. (EU-SIPCO)*, Sep 2013, pp. 1–5.

- [16] A. A. Kumar, S. G. Razul, and C. M. S. See, "An efficient sub-Nyquist receiver architecture for spectrum blind reconstruction and direction of arrival estimation," in *Proc. IEEE Int. Conf. on Acous. Speech and Signal Process. (ICASSP)*, May 2014, pp. 6781–6785.
- [17] —, "Spectrum blind reconstruction and direction of arrival estimation at sub-Nyquist sampling rates with uniform linear array," in *Proc. IEEE Int. Conf. Digital Sig. Process. (DSP)*, July 2015, pp. 670–674.
- [18] S. Stein, O. Yair, D. Cohen, and Y. C. Eldar, "Joint spectrum sensing and direction of arrival recovery from sub-Nyquist samples," in *Proc. IEEE Signal Process. Adv. Wireless Commun.(SPAWC)*, June 2015, pp. 331–335.
- [19] L. Liu and P. Wei, "Joint DOA and frequency estimation with sub-Nyquist sampling," *arXiv preprint arXiv:1604.05037*, Apr 2016.

